# Robust Price-based EV Load Management Considering Human-choice Uncertainty

Weile Kong, *Student Member, IEEE*, Hongxing Ye, *Senior Member, IEEE*, Yinyin Ge, *Member, IEEE*,

*Abstract*—This paper presents a robust bi-level optimization model with near-optimal solution in lower-level to manage the electric vehicle (EV) load. The diversity of human preferences gives rise to uncertain human-choices when multiple options share the same charging cost. This uncertainty contributes to markedly distinct load profiles, resulting in severe ramping events, congestion, and voltage issues. To address it, this paper proposes a Location-Time-of-Use (LToU) charging price-based EV demand management approach that aims to flatten the net load curve in the face of uncertainties related to human choices. It is important to note that EV owners may have multiple near-optimal solutions to choose from, resulting in different demand response profiles. Therefore, it is essential to model EV owner's choice uncertainties, so that LToU rate can be correctly set. Addressing lower-level solution uncertainty in optimization models remains an open question in the literature. This work aims to bridge the gap with the proposed model. By exploring the model structure, we propose a group of optimality conditions and an algorithm to solve the problem. We perform comprehensive simulations with a power-transportation system. The results show the proposed approach can help flatten the load curve under human-choice uncertainty.

*Index Terms*—Pricing, Uncertainty, Demand Management, Electric Vehicle

## NOMENCLATURE

### Functions

| | |
|---|---|
| $C_{n,k,t}(\pi)$ | Charging cost in function of charging rate |
| $f(\boldsymbol{P})$ | Objective in function of power generation |
| $P_{i,t}^{load}(\pi)$ | Real demand in function of charging rate |
| $Q_{i,t}^{load}(\pi)$ | Reactive load in function of charging rate |

### Indices

| | |
|---|---|
| $(i,j)/i,j/t$ | Index of branch/node in PDN/time slot |
| $g/k/n/r$ | Index of generator/FCS/EV/PV |
| $l$ | Index of segment of piecewise function |
| $s$ | Index of discrete charging price segment |

### Parameters

| | |
|---|---|
| $\alpha/\beta/\gamma$ | Cost weight of charging rate, distance and plug-in time discomfort degree |
| $\bar{\pi}_k/\bar{\pi}_t$ | Mean charging rate at FCS $k$/time slot $t$ |
| $\delta_n$ | Acceptable cost increment for customer $n$ |
| $\eta_{n,t}$ | Plug-in time discomfort degree of EV $n$ charging at time slot $t$ |
| $\hat{\pi}_{k,t,s}$ | Price map representing the $s$th price choice of FCS $k$ at time slot $t$ |
| $\pi_{k,min}/\pi_{k,max}$ | Minimum/maximum charging rate at FCS $k$ |
| $\tilde{\theta}_{ij,t}$ | Phase difference between node $i$ and $j$ at time $t$ attained from last iteration |

W. Kong, H. Ye, and Y. Ge are with Xi'an Jiaotong University, Xi'an, 710049, China (e-mail: k1500304829@stu.xjtu.edu.cn; yehxing@xjtu.edu.cn; geyinyin@xjtu.edu.cn). Hongxing Ye is the corresponding author.

| | |
|---|---|
| $\tilde{v}_{i,t}$ | Voltage magnitude of node $i$ at time $t$ attained from last iteration |
| $b_{ij}/g_{ij}$ | Susceptance/conductance of branch $(i,j)$ |
| $E_n$ | Energy demand of EV $n$ |
| $P_n$ | Charging power of EV $n$ |
| $P_{g,min}^{gen}/P_{g,max}^{gen}$ | Real power bounds of generator $g$ |
| $p_{l,g}^{seg}$ | Length of segment $l$ |
| $Q_{g,min}^{gen}/Q_{g,max}^{gen}$ | Reactive power bounds of generator $g$ |
| $T_{n,t}^{tr}$ | Travelling time of EV $n$ to FCS $k$ |
| $v_{i,min}/v_{i,max}$ | Voltage magnitude bounds at node $i$ |

### Sets

| | |
|---|---|
| $\mathcal{B}/\mathcal{N}/\mathcal{T}$ | Set of all branches//nodes in PDN/time slots |
| $\mathcal{B}(i)/\mathcal{K}(i)$ | Set of branches/FCSs connected to node $i$ |
| $\mathcal{E}/\mathcal{G}/\mathcal{K}/\mathcal{R}$ | Set of EVs/generators/FCSs/PVs |
| $\mathcal{G}(i)/\mathcal{R}(i)$ | Set of generators/PVs connected to node $i$ |
| $\mathcal{S}$ | Set of discrete charging price segments |

### Variables

| | |
|---|---|
| $\mu_{n,k,t}$ | Dual variable of constraint (29) |
| $\pi_{k,t}$ | Charging rate of FCS $k$ at time $t$ |
| $\theta_{ij,t}$ | Voltage phase difference between node $i$ and $j$ at time $t$ |
| $\varphi_{n,k,t}$ | Auxiliary variable for bi-linear component $\mu_{n,k,t}\pi_{k,t}$ |
| $I_{n,k,t}$ | EV charging selection indicator, 1 for selected and 0 otherwise |
| $P_{g,t}^{gen}/Q_{g,,t}^{gen}$ | Real/Reactive power generation of generator $g$ at time $t$ |
| $P_{i,t}^{cs}$ | EV charging load of node $i$ at time slot $t$ |
| $P_{i,t}^{load}/Q_{i,t}^{load}$ | Real/Reactive power demand of node $i$ at time $t$ |
| $P_{ij,t}^{line}/Q_{ij,s,t}^{line}$ | Real/Reactive power flow of branch $(i,j)$ at time $t$ |
| $U_{k,t,s}$ | Charging price choice indicator, 1 for selecting $s$th price segment and 0 otherwise |
| $v_{i,t}$ | Voltage magnitude of node $i$ at time $t$ |

## I. INTRODUCTION

GREENHOUSE gas emissions have received significant attention in recent years. As the two largest contributors, the transportation and power sectors are accountable for 37.7% and 27.5% of the U.S.'s fossil fuel in 2022 [1]. These two sectors account for over 65% of global primary energy consumption worldwide. As a countermeasure, transportation electrification has been recognized as a potential solution given its ecologically friendly and cost-efficient advantages.

In the transportation sector, EVs as the substitute of internal combustion engine (ICE) vehicles have seen great devel-

opment. Following a decade of rapid growth, the sales of EVs exceeds 10 million in 2022 [2]. 230 million EVs are projected to hit the load by 2030 in the supportive policy of net zero-emission scenario [2]. Meanwhile, the ever-increasing adoption of EVs has a strong demand for advanced battery technology and smart charging infrastructure networks. To meet this demand, public charging stations, equipped with charging piles that connect EVs to the power grid, have been rapidly deployed. At the end of 2022, publicly accessible charging points have reached 1.76 million in China, with fast chargers accounting for 43.2% of the total [2]. This extensive charging infrastructure serves as a vital link between the power and transportation systems. Large-scale fast-charging stations (FCSs) could easily create a peak load in power systems, posing challenges to system stability. As the integration of EVs accelerates, uncoordinated simultaneous connection and charging may lead to elevated peaks, causing various adverse effects on power distribution networks (PDNs).

Charging rate, distance, and plug-in time are main concerns for EV owners when making charging choices [3]. Generally, EV owners exhibit rational behavior by selecting the nearest FCS with a lower charging rate to align with their preferences [4]. The uncontrolled individual behavior may cause congestion in both FCS and PDN [5]. Notably, congestion in the coupled systems is interdependent, meaning that congestion in PDN can influence the charging rate adjustment in FCS. Price-sensitive customers may opt for different FCSs, thereby mitigating the burden on PDN caused by charging loads [6]. Moreover, it can aid in the redistribution of traffic within transportation networks [7]. Furthermore, EVs are well-known partially flexible loads in the demand response program [8], which is also a kind of spatial-temporal shiftable battery storage. It is essential to study the spatial-temporal scheduling of EVs in load management. A real-time smart EV charging scheme based on the data metering is proposed in [9], generating control signals for peak shaving in commercial and industrial districts. At the apartment level, a centralized EV charging scheduling method is proposed in [10] with comprehensive information, achieving peak load reduction and charging cost savings. Taking into account the charging urgency indicator, a coordinated EV scheduling model is developed in [11] to mitigate the peak-valley load difference. Moreover, a customer feedback-based peak load management model is established in [12], considering various spatial-temporal EV penetrations. In the pursuit of flattening the peak load and minimizing operational costs in [13], a bi-objective multi-depot EV scheduling problem is formulated and solved using a tailored branch-and-price approach. Notably, this study suggests that EV customers exhibit sensitivity to high-tariff periods. Therefore, properly pricing the charging service becomes instrumental in optimizing the operation of the integrated power-transportation system [14].

Many studies have explored different incentive approaches to manage the EV load. A geographically variant electricity prices scheme is proposed in [15] to influence EV charging patterns and maximize the utilization of FCSs simultaneously. To mitigate FCS congestion, pricing dynamics are applied in [16] considering the occurrence of loss of load events. In our previous work, a dynamic pricing scheme is proposed to manage the EV load without considering uncertainty [17]. Besides, the menu-based pricing method is proposed in [18] to manage EVs only considering the route uncertainty. To tackle uncertainties of charging demand volatility, inherent intermittency of renewable energy generation, and wholesale electricity price fluctuation, stochastic dynamic programming and greedy algorithms are utilized to determine suitable charging rates and manage electricity in [19]. Aim at maximizing the profit of EV private charging stations, optimal EV charging coordination and pricing mechanisms are proposed to coordinate the operation of distributed EV charging stations and PV farms considering the uncertainties of PV output power and electricity prices in [20]. Time-of-Use (ToU) rate is also effective on EV charging scheduling and peak shaving [21], [22]. The aforementioned uncertainties primarily pertain to continuous aspects such as price, renewable output, arrival patterns, and demand. However, uncertainties associated with binary human decisions have been overlooked.

Due to the unique relationship between FCSs and EVs, the problem typically exhibits a hierarchical structure, particularly a bi-level structure [23]. Numerous researchers have dedicated their efforts to tackling the bilevel problem. From a pure optimization standpoint, a column-and-constraint generation (CCG) method is devised after reformulating the bilevel program into a single-level program in [24] to address the bilevel mixed-integer program (MIP) within finite iterations. By decomposing the bilevel problem into a first-stage IP and a second-stage MIP, a generalized value function method is introduced in [25] to solve stochastic and bilevel MIP. In the realm of bilevel robust unit commitment, a Benders decomposition-based method is proposed in [26]. Notably, these methods predominantly focus on the optimistic bilevel formulation. Adopting a data-optimization hybrid perspective, a reinforcement learning-based approach is proposed in [27] to address bilevel voltage regulation in distribution systems. Furthermore, an offline value function calculation and online schedule-combined bilevel energy management strategy are introduced in [28] to handle EV loads under probabilistic traffic patterns. In [29], a bilevel price-based demand-side energy management problem is solved by a learning-based optimization method. However, it is worth noting that these learning-based methods entail prolonged offline training times and possess limited generalization abilities.

However, incorporating human-choice rationality and solution multiplicity at the lower level makes it a challenging problem with pessimistic characteristics. For instance, in scenarios where multiple options entail the same charging cost accounting for human-choice uncertainty, the accumulation of charging power may occur at a particular FCS during a time slot. This accumulation substantially amplifies the peak-valley difference, giving rise to challenges such as ramping burden [30], power congestion [31], and voltage deviation [32] within the power system. Some existing literature is concentrated on addressing the pessimistic bi-level problem. When the lower-level problem is convex, a duality-based robust solution method is proposed for the bi-level problem [33]. In [34], a tight relaxation of the pessimistic bilevel

problem is introduced, for the problem with special structure. It is still hard to solve the bi-level problem with a pure integer lower-level problem for lacking dual information. In this work, we propose a Successive Scenario Generation algorithm to solve the bilevel problem. The most relevant to our work is CCG [35], but the distinct differences from them are: 1) CCG systematically generates and incorporates decision variables and constraints into the master problem gradually by identifying and including significant scenarios, obtaining an optimal solution within a fixed, finite, discrete uncertainty set. 2) SSG serves as a heuristic optimization method, yielding a local optimum with a decision-dependent uncertainty set. Our objective is to determine the time- and location-varying prices to balance spatiotemporal load using the worst-case scenario that causes the peak load. If scenarios are added gradually, feasible prices may be compelled into a flat line throughout the day, contrary to our goal of guiding charging through time- and location-varying prices. Consequently, we propose SSG, which adds only one scenario to the master problem and removes the corresponding constraints from the last iteration.

Human-choice uncertainty is a challenging topic in the demand response literature. Even a rational EV owner makes an FCS-selection decision with uncertainty to some extent, as it is hard to define the "optimal" choice considering human preferences. FCS selection uncertainty can result in large step-wise load differences in the upper level. To fill the research gap, we study the coordinated operation between PDN and FCSs considering human FCS selection uncertainty, which aims at addressing the open question of our earlier work [17]. The incorporation of geographical location information plays a pivotal role in diverse price settings and enables unified spatial and temporal load balancing [36], [37]. In this study, we harness both the geographic and temporal variations of charging prices to mitigate operational costs and achieve a flattened netload. This paper proposes robust a bi-level model and solution approach to determining the Location-Time-of-Use (LToU) charging rate, extending the Time-of-Use rate with location information. The main contributions are threefold.

- Human-choice uncertainty is integrated into the robust bi-level EV load management model, which is ignored in most literature. By adjusting LToU charging rate in the upper level, we leverage the EV load response to flatten the load curve. However, due to lower level solution multiplicity and inner characteristics, uncertain charging choices can lead to significantly different load profiles. Hence, it is fundamentally important to consider the human-choice uncertainties. We also conduct an exploratory survey in the City of Xi'an, providing a comprehensive analysis of EV owners' preferences.
- A novel solution approach is proposed to solve the robust bi-level optimization model with solution near-optimality and multiplicity in the lower level. First, it is challenging to solve the original bi-level problem with a non-convex integer model at the lower level. We propose a group of novel optimality conditions, reducing the optimality constraint (OC) number from $\mathcal{O}(n^2)$ to $\mathcal{O}(n)$. Second, the optimality gap and solution multiplicity for human-choice
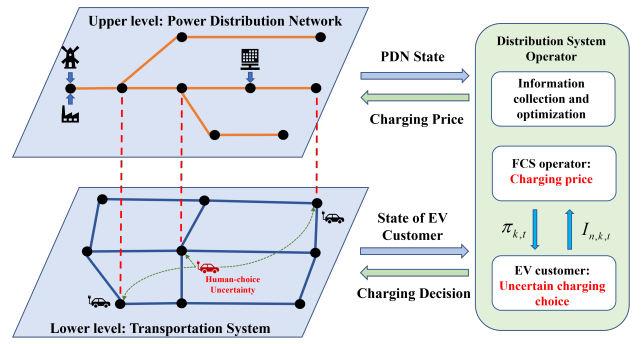


Fig. 1. The upper-level problem is an optimal power flow model that determines the LToU charging rate for each FCS. The lower level problem is to select the near-optimal FCS considering the **human choice uncertainty**.

uncertainty further complicate the problem. By exploiting the problem structure, we propose a successive scenario generation algorithm to find the local optimal solution.
- This work reveals the limitation of price-based EV load management. By conducting a comprehensive case study, it is found capability of price-based load management is restrained by price feasible region, user rationality, and solution multiplicity. Price-based EV load management can help reshape the load curve to a certain extent, not any desired curve even if all EVs respond to the price.

The remainder of this paper is organized as follows. Section II introduces a bi-level EV load management model considering human-choice uncertainty. A robust iterative solution approach is proposed in Section III. In Section IV, case studies are conducted and the results are analyzed in detail. Finally, conclusions are drawn in section V with potential future work.

## II. MATHEMATICAL MODEL

This work primarily focuses on addressing the human-choice uncertainty model and developing an algorithm to tackle the issue of solution multiplicity. As a result, the charging process and transportation model are simplified for the purpose of the study. Before we establish the bi-level model, the assumptions used in this work are presented as follows.

- Utilities coordinate with FCS operators. For example, The E.ON group in Germany is one of Europe's largest operators of fast-charging networks and energy infrastructure. State Grid China owns and operates a large volume of FCSs.
- EV owners charge at the FCS via APP, which gives the FCS operator access to EV's location, battery capacity, and SOC. The FCS operator can acquire the approximate EV load demand within an area. EV owners can access information about available charging piles and make appointments.
- The charging process for electric vehicles is simplified and does not consider complex factors such as vehicle-to-grid interactions, bidirectional charging, or advanced charging strategies. Instead, a basic representation of the charging process is used, which assumes a single charging

rate per period and a single time slot and FCS to finish the charging activity.

- The transportation model is also simplified and does not consider detailed aspects such as traffic congestion, routing optimization, or vehicle dynamics. Instead, a simplified representation of the transportation system is used, focusing on the load impact of electric vehicles and their charging profiles.

Fig. 1 illustrates the main idea of the proposed bi-level programming model. The upper level is an optimal power flow model aiming to flatten the net load profile and reduce the total operation cost based on LToU pricing. The lower level is a charging FCS and plug-in time selection model with human-choice uncertainty whose results form the demand in the upper level.

This section first presents an abstract form of the bi-level model. Then, we detail an optimal power flow model for PDN and FCS selection model for EV. The abstract form of the bi-level model can be formulated as

$$(P1): \min_{x,\pi} \max_{\delta \in \mathcal{U}} \quad c^T x$$
$$\text{s.t.} \quad Ax + Dy + G\pi \le b$$
$$y \in \Big\{ y : f_n(y_n, \pi) \le z_n^* + \delta_n,$$
$$z_n^* = \min_{y_n \in \mathcal{D}_n} f_n(y_n, \pi), \forall n \Big\},$$

where $x$ denotes the continuous variables representing the nodal power and voltage in the optimal power flow problem and $\pi$ represents the LToU charging rate. $y$ denotes the integer variables for the (near) optimal charging decisions for EVs. $z_n^*$ is the optimal objective value for EV $n$ with least cost. $\delta_n$ represents the human-choice uncertainty in this work. $f_n(y_n, \pi)$ represents the charging objective of user $n$. $\mathcal{D}_n$ is the lower level feasible region of EV $n$. Other symbols are the corresponding coefficients. For instance, let $c$ denote the coefficient vector associated with nodal power and voltage, where $c^T x$ represents the objective function of the upper-level problem encompassing the total operational cost. Matrices $A$, $D$, and $G$ are the coefficient matrices for power and voltage variables, charging indicator variables, and charging price variables, respectively. The inequality $Ax + Dy + G\pi \le b$ encapsulates the constraints of the upper-level problem, incorporating power flow and price limits. $f_n(y_n, \pi) \le z_n^* + \delta_n$ represents the charging selection constraint under human-choice uncertainty $\delta_n$.

### A. Human Preference and Choice Uncertainty

Before introducing the detailed bi-level optimization model, we give a detailed description about how to model the human-choice uncertainty. In practice, the majority of EV owners prioritize the comfort and satisfaction of the charging service. Therefore, human preferences for EV charging differ among customers and are characterized by cost weights $(\alpha, \beta, \gamma)$ assigned to charging rate, distance, and plug-in time in the proposed model. These varying cost weights contribute to distinct optimal conditions and significantly impact load management. Consequently, estimating an EV customer's charging

preference is crucial for managing the charging load through appropriate LToU charging rates. To comprehensively analyze EV owners' attitudes towards charging rate, distance, and plug-in time discomfort degree, we conduct an exploratory survey using a paper-based questionnaire, which includes numerical rating questions for each factor.

Generally, most EV owners prefer charging at the FCS offering the minimum overall cost. The optimal value function is defined as (1).

$$y \in \arg \min_{y_n \in \mathcal{D}_n} \Big\{ f_n(y_n, \pi), \forall n \Big\}$$
$$z_n^* = \min_{y_n \in \mathcal{D}_n} f_n(y_n, \pi), \forall n \qquad (1)$$

However, for a feasible upper-level decision, LToU charging rate, the solution $y_n$ to the lower level is not unique. Besides, due to human preference, some EV owners may forgo charging at the FCS with minimum overall cost in exchange for a slight cost increase $\delta_n$ for specific reasons, referred to as ***human-choice uncertainty***. To protect itself against possible follower deviations from its optimality, we seek a decision $\pi$ at the upper level that is robust in the sense that it remains near-optimal or good enough even if the lower level deviates from its optimality. We then formulate the near-optimal set $\mathcal{Z}(\pi, \delta_n)$ of the lower level as follows.

$$\mathcal{Z}(\pi, \delta_n) = \Big\{ y : f_n(y_n, \pi) \le z_n^* + \delta_n \Big\}$$

### B. Upper-level Problem

The upper-level problem is a special optimal power flow problem, whose load is a (near) optimal solution to a lower-level FCS selection problem. The objective of the upper-level problem aims to minimize the total operation costs of PDN in the whole day. It can also flatten the net load by applying the stair-like electricity price. The piecewise linear cost function $f(p)$ is divided by points $\{0, p_{1,g}^{seg}, \cdots, p_{L,g}^{seg}\}$, which can be formulated by either binary variables or special ordered sets of type 2 (SOS2) [38]. By introducing continuous $w_{l,g,t}$ and binary variables $u_{l,g,t}$, the objective function of upper-level problem can be described as

$$f(\boldsymbol{P}) = \sum_{l=1}^{L+1} \sum_{g=1}^{|\mathcal{G}|} \sum_{t=1}^{T} w_{l,g,t} f(p_{l,g}^{seg}), \qquad (2)$$

with

$$P_{g,t}^{gen} = \sum_{l=1}^{L+1} w_{l,g,t} p_{l,g}^{\text{seg}}, \ \forall t \in \mathcal{T}, \forall g \in \mathcal{G}, \qquad (3)$$
$$w_{1,g,t} \le u_{1,g,t}, \ w_{2,g,t} \le u_{1,g,t} + u_{2,g,t}, \ \cdots, \qquad (4)$$
$$w_{n,g,t} \le u_{L-1,g,t} + u_{L,g,t}, \ w_{L+1,g,t} \le u_{L,g,t}, \qquad (5)$$
$$w_{1,g,t} + w_{2,g,t} + \cdots + w_{L+1,g,t} \le 1, \qquad (6)$$
$$u_{1,g,t} + u_{2,g,t} + \cdots + u_{L,g,t} \le 1. \qquad (7)$$

In this work, we focus on the FCS pricing scheme and human-choice uncertainty. Thus, an iterative linearized OPF model from [39] is employed to represent the power flow with a good tradeoff between computational efficiency and accuracy. The uncertain EV load is a function of the LToU

rate which is also determined here. Then, the model is built as follows.

$$\sum_{g\in\mathcal{G}(i)} P_{g,t}^{gen} + \sum_{r\in\mathcal{R}(i)} P_{r,t}^{pv} - P_{i,t}^{load}(\pi) = \sum_{(i,j)\in\mathcal{B}(i)} P_{ij,t}^{line}, \forall i,t \quad (8)$$

$$\sum_{g\in\mathcal{G}(i)} Q_{g,t}^{gen} - Q_{i,t}^{load}(\pi) = \sum_{(i,j)\in\mathcal{B}(i)} Q_{ij,t}^{line}, \forall i,t \quad (9)$$

$$P_{ij,t}^{line} = g_{ij}\left(\frac{v_{i,t}^2 - v_{j,t}^2}{2} + \tilde{\theta}_{ij,t}\theta_{ij,t} - \frac{1}{2}\tilde{\theta}_{ij,t}^2\right) - b_{ij}\theta_{ij,t}$$
$$+ \left[g_{ij}\frac{\tilde{v}_{i,t} - \tilde{v}_{j,t}}{\tilde{v}_{i,t} + \tilde{v}_{j,t}}\left(v_{i,t}^2 - v_{j,t}^2\right) + \frac{g_{ij}}{2}\left(\tilde{v}_{i,t}^2 - \tilde{v}_{j,t}^2\right)^2\right] \quad (10)$$

$$Q_{ij,t}^{line} = b_{ij}\left(\frac{v_{j,t}^2 - v_{i,t}^2}{2} - \tilde{\theta}_{ij,t}\theta_{ij,t} + \frac{1}{2}\tilde{\theta}_{ij,t}^2\right) - g_{ij}\theta_{ij,t}$$
$$- \left[b_{ij}\frac{\tilde{v}_{i,t} - \tilde{v}_{j,t}}{\tilde{v}_{i,t} + \tilde{v}_{j,t}}\left(v_{i,t}^2 - v_{j,t}^2\right) + \frac{b_{ij}}{2}\left(\tilde{v}_{i,t}^2 - \tilde{v}_{j,t}^2\right)^2\right] \quad (11)$$

$$P_{g,\min}^{gen} \le P_{g,t}^{gen} \le P_{g,\max}^{gen}, \ \forall g,t \quad (12)$$

$$Q_{g,\min}^{gen} \le Q_{g,t}^{gen} \le Q_{g,\max}^{gen}, \ \forall g,t \quad (13)$$

$$v_{i,\min}^2 \le v_{i,s,t}^2 \le v_{i,\max}^2, \quad \forall i,t \quad (14)$$

$$\frac{1}{T}\sum_{t\in\mathcal{T}} \pi_{k,t} = \bar{\pi}_k, \ \forall k \quad (15)$$

$$\pi_{k,t} = \sum_{s\in\mathcal{S}} U_{k,t,s}\hat{\pi}_{k,t,s} \quad (16)$$

$$\sum_{s\in\mathcal{S}} U_{k,t,s} = \mathbf{1}, \forall k,t \quad (17)$$

$$\pi_{k,\min} \le \pi_{k,t} \le \pi_{k,\max}, \ \forall k,t \quad (18)$$

$$\Delta\pi_{k,\min} \le \pi_{k,t+1} - \pi_{k,t} \le \Delta\pi_{k,\max}, \ \forall k \quad (19)$$

The nodal active and reactive power balance equations are formulated as (8) and (9). Equation (10) and (11) are linear active and reactive power flow constraints by regarding $v_{i,t}^2$ as a new independent variable. The capacity of active and reactive power for generators is denoted by (12) and (13). Voltage magnitude is bounded in (14). Apart from the electrical constraints, it is practical to enforce regulation constraints on charging rates in oligopoly markets. Therefore, we consider that the average price of each FCS for the whole day is fixed in equation (15). Equations (16) and (17) denote the process by which the charging price is determined from a discrete price map, ensuring the selection of only one price per FCS during each time slot. At the same time, each FCS's charging rate should be bounded within a range (18). Besides, to prevent the dramatic price variations, constraints (19) is applied. As a side note, one could alter the regulatory constraints.

### C. Lower-level Problem

In the lower-level problem, it is assumed that EV owners act rationally, selecting FCS based on factors such as charging rate, distance, and plug-in time preference. Charging rates are assumed to be publicly accessible for all EVs within a specific area. Consequently, the lower-level objective function includes charging fees, distance, and plug-in time discomfort degree. Based on the human-choice uncertainty and near-optimal set detailed in Section II-A, the lower-level model

is thus formulated as follows.

$$I_{n,k,t} \in \left\{ \boldsymbol{I}: \sum_{k=1}^{K}\sum_{t=1}^{T} C_{n,k,t}(\pi)I_{n,k,t} \le C_n^* + \delta_n \right. \quad (20)$$

$$C_n^* = \min_{I_{n,k,t}} \sum_{k=1}^{K}\sum_{t=1}^{T} C_{n,k,t}(\pi)I_{n,k,t} \quad (21)$$

$$C_{n,k,t}(\pi) = \alpha\pi_{k,t}E_n + \beta T_{n,k}^{tr} + \gamma\eta_{n,t} \quad (22)$$

$$\left. \sum_{t=1}^{T}\sum_{k=1}^{K} I_{n,k,t} = \mathbf{1}, \quad \forall n\in\mathcal{E} \right\} \quad (23)$$

The binary variable $I_{n,k,t}$ is a selection indicator, with $I_{n,k,t} = 1$ if EV $n$ chooses to charge at FCS $k$ at time slot $t$, and 0 otherwise. Constraint (20) signifies that EV owners opt for a near-optimal FCS. Equation (21) seeks the least objective value $C_n^*$ for each EV customer. The objective value of EV $n$ charging at FCS $k$ during time $t$ is denoted by $C_{n,k,t}(\pi)$ and comprises three components including charging fee, distance cost, and plug-in time discomfort, as illustrated in equation (22). Equation (23) ensures that each EV is charged only once finished in one FCS, preventing multiple charging sessions within a single time slot. By considering equation (23), the study aims to accurately represent the charging behavior, i.e. human-choice uncertainty. However, it is important to note that these assumptions should be carefully considered in real-world applications including charger allocation and waiting scenes.

### D. Bi-level Programming Model

The EV load is an aggregation of the charging demand for all EVs at each node. As demonstrated in (20)-(23), EV charging choice is a function of charging rate, distance, and the discomfort degree associated with plug-in time. The EV charging load at node $i$ is defined as

$$P_{i,t}^{cs} = \sum_{k\in\mathcal{K}(i)}\sum_{n\in\mathcal{E}} I_{n,k,t}P_n, \quad (24)$$

where $\mathcal{K}(i)$ is set of all FCSs located at node $i$, and $\mathcal{E}$ is set of all EVs. Accordingly, the total load at node $i$ is

$$P_{i,t}^{load}(\pi) = P_{i,t}^d + P_{i,t}^{cs}. \quad (25)$$

Finally, a robust bi-level programming model is formulated as

$$\begin{aligned} (\text{P2}): \min_{\pi}\max_{I} \quad & f(\boldsymbol{P}) \\ \text{s.t.} \quad & (3)\text{-}(19),(24),(25) \\ & I_{n,k,t} \in \left\{(20)\text{-}(23)\right\}. \end{aligned}$$

### III. Solution Methodology

This section presents an approach to solve the proposed robust bi-level model. First, we establish near-optimal conditions for the lower-level problem and recast the original pessimistic bi-level programming model into a robust 'min-max' mixed-integer linear programming (MILP) model. Then, the novel successive scenario generation method is proposed to find the local optimal solution.

## A. Near-optimality Condition

The main difficulty is the user rationality and solution multiplicity in the lower-level problem. In order to consider human-choice uncertainty, we model a feasible region in the lower level rather than a single optimal point. Therefore, we propose to establish a group of conditions to represent the lower-level FCS selection problem solutions.

**Proposition 1.** $C_{n,k,t}(\pi)$ *in* (22) *is the minimum objective value for EV n, if and only if*

$$C_{n,k,t}(\pi)I_{n,k,t} \le C_{n,k',t'}(\pi), \forall k' \in \mathcal{K}\backslash k, t' \in \mathcal{T}\backslash t, \quad (26)$$
$$\sum_{t \in \mathcal{T}}\sum_{k \in \mathcal{K}} I_{n,k,t} = \mathbf{1}.$$

Constraint (26) ensures the optimal objective and choice of EV owners in the lower-level problem. By employing the big-M method, the optimality condition is reformulated as

$$C_{n,k,t}(\pi) \le C_{n,k',t'}(\pi) + (1-I_{n,k,t})M, \forall k' \in \mathcal{K}\backslash k, t' \in \mathcal{T}\backslash t \quad (27)$$
$$\sum_{t \in \mathcal{T}}\sum_{k \in \mathcal{K}} I_{n,k,t} = \mathbf{1}.$$

These optimality conditions are computationally expensive. The computational complexity is $O(|\mathcal{K}|^2|\mathcal{T}|^2)$. To address this problem, we propose a novel group of optimality conditions whose computational complexity is $O(|\mathcal{K}||\mathcal{T}|)$. Let $z_n$ represent an auxiliary variable, with its optimal value denoting the minimum cost of EV $n$. The lower level problem (21)-(23) is equivalent to

$$\max_{z_n} \; z_n \quad (28)$$
$$\text{s.t.} \; z_n \le \alpha\pi_{k,t}E_n + \beta T_{n,k}^{tr} + \gamma\eta_{n,t}, \forall k \in \mathcal{K}, t \in \mathcal{T}. \quad (29)$$

The dual of the above problem is written as

$$\min_{\mu_{n,k,t}} \sum_{k=1}^{K}\sum_{t=1}^{T} \mu_{n,k,t}(\alpha\pi_{k,t}E_n + \beta T_{n,k}^{tr} + \gamma\eta_{n,t}) \quad (30)$$
$$\text{s.t.} \; \sum_{k=1}^{K}\sum_{t=1}^{T} \mu_{n,k,t} = 1 \quad (31)$$
$$\mu_{n,k,t} \ge 0, \; \forall k \in \mathcal{K}, t \in \mathcal{T}, n \in \mathcal{N}, \quad (32)$$

in which, $\mu_{n,k,t}$ serves as the dual variable for constraint (29), while equation (31) represents the constraint in the dual problem for the auxiliary variable $z_n$. According to the strong duality of the linear programming problem, we have the proposition below.

**Proposition 2.** *The optimal solution to problem* (28)-(29) *is attained if and only if*

$$z_n = \sum_{k=1}^{K}\sum_{t=1}^{T} \mu_{n,k,t}(\alpha\pi_{k,t}E_n + \beta T_{n,k}^{tr} + \gamma\eta_{n,t}), \quad (33)$$
$$z_n \le \alpha\pi_{k,t}E_n + \beta T_{n,k}^{tr} + \gamma\eta_{n,t}, \; \forall k \in \mathcal{K}, t \in \mathcal{T}, \quad (34)$$
$$\sum_{k=1}^{K}\sum_{t=1}^{T} \mu_{n,k,t} = 1, \quad (35)$$
$$\mu_{n,k,t} \ge 0, \; \forall k \in \mathcal{K}, t \in \mathcal{T}, n \in \mathcal{N}. \quad (36)$$

We observe that $\mu_{n,k,t}$ always takes values of either 0 or 1. As a result, equation (33) consistently holds, allowing $\mu_{n,k,t}$

to be replaced by the binary variable $I_{n,k,t}$. In other words, the dual problem (30)-(32) is equivalent to the primal problem (28)-(29).

By establishing the optimality conditions and substituting $\mu_{n,k,t}$ with the binary variable $I_{n,k,t}$, the lower-level problem incorporating human-choice uncertainty is reformulated as a set of constraints. For a given upper-level decision $\pi$ and optimality tolerance $\delta_n$, EV owners may choose any option in the feasible region from the proposition below.

**Proposition 3.** *The original lower level charging selection problem* (20)-(23) *is equivalent to the following **near-optimality conditions**.*

$$\mathbf{I}:\begin{cases} \sum_{k=1}^{K}\sum_{t=1}^{T} I_{n,k,t}(\alpha\pi_{k,t}E_n + \beta T_{n,k}^{tr} + \gamma\eta_{n,t}) \le z_n + \delta_n & (37) \\[2mm] z_n \le \alpha\pi_{k,t}E_n + \beta T_{n,k}^{tr} + \gamma\eta_{n,t}, \forall k \in \mathcal{K}, t \in \mathcal{T} & (38) \\[2mm] \sum_{k=1}^{K}\sum_{t=1}^{T} I_{n,k,t} = 1 & (39) \\[2mm] I_{n,k,t} \in \{0,1\}, \; \forall k \in \mathcal{K}, t \in \mathcal{T}, n \in \mathcal{N} \end{cases} \quad (40)$$

There are bi-linear terms $I_{n,k,t}\pi_{k,t}$ in (37), which can be linearized by auxiliary variable $\varphi_{n,k,t}$ with linearization constraints

$$(I_{n,k,t} - 1)\pi_{k,max} + \pi_{k,t} \le \varphi_{n,k,t} \le \pi_{k,t}, \quad (41)$$
$$I_{n,k,t}\pi_{k,min} \le \varphi_{n,k,t} \le I_{n,k,t}\pi_{k,max}, \quad (42)$$
$$I_{n,k,t} \in \{0,1\}. \quad (43)$$

The original robust bi-level programming model is then recast as a novel robust "min-max" model.

$$(\text{P3}): \min_{\pi}\max_{I} \; f(\boldsymbol{P})$$
$$\text{s.t.} \quad (3)\text{-}(19),(24),(25),(37)\text{-}(39),(41)\text{-}(43)$$

## B. Successive Scenario Generation Method

Although near-optimality conditions are established, the solution multiplicity of lower-level problem causes the difficulty. It is hard to solve because of the mixed integer structure and pure integer-related objective [24]. To overcome the above problem, we present a successive scenario generation (SSG) method. The main idea is to find a near-optimal solution considering the optimality gap between the worst and best-case scenarios. The best-case scenario (MP) and worst-case scenario (SP) are solved iteratively. Specifically, the two objectives are opposite. The main goal of the (MP) is to identify the most efficient charging prices for FCSs, minimizing the utility's operational costs. On the other hand, the SP is formulated to determine the least favorable charging choices for uncontrollable EVs, ultimately maximizing the utility's operational costs.

Algorithm 1 summarizes the iterative solution process for the best-case problem (MP) and worst-case problem (SP). The LToU charging rate is updated using the worst-case charging load information obtained from the solution to SP. In which,

$\Phi, \Phi_b^{(i)}$, and $\Phi_w^{(i)}$ are sets of all EVs, controllable EVs, and the top $N_s$ worst uncontrollable EVs.

$$(\text{MP}): Z^{lb} = \min_{\pi} f(\boldsymbol{P})$$
$$\text{s.t. } (3)\text{-}(19),(24),(25),(37)\text{-}(39),(41)\text{-}(43)$$
$$I_{n,k,t} = I_{n,k,t}^{(i-1)}, \forall n \in \Phi_w^{(i-1)}, k, t \quad (44)$$
$$I_{n,k,t} \in \{0,1\}, \forall n \notin \Phi_w^{(i-1)}, k, t \quad (45)$$

$$(\text{SP}): Z^{ub} = \max_{I} f(\boldsymbol{P})$$
$$\text{s.t. } (3)\text{-}(19),(24),(25),(37)\text{-}(39),(41)\text{-}(43)$$
$$I_{n,k,t} \in \{0,1\}, \ \forall n, k, t \quad (46)$$
$$\pi_{k,t} = \pi_{k,t}^{(i-1)}, \ \forall k, t \quad (47)$$

Upon analyzing the problem structure, it becomes apparent that the behaviors of each EV in problem SP are independent once the charging prices are determined in the MP problem. This observation allows for the deconstruction of the SP into subproblems for each individual EV. Within each EV subproblem, the set of charging choices can be derived via a closed-form equation and subsequent sorting of costs across all FCSs and time slots. This decentralized approach exhibits commendable performance, especially in terms of scalability when applied to large-scale problems.

**Proposition 4.** *Let $Z^*$ be the global optimal value of problem (P3), then $Z^{lb}$ is a lower bound of $Z^*$, and $Z^{ub}$ is an upper bound of $Z^*$. An acceptable solution $\pi_{k,t}^*$ is attained when Algorithm 1 converges, and the optimality gap*

$$Z^{ub} - Z^* \leq \Delta. \quad (48)$$

*Proof.* The LToU charging rate $\pi_{k,t}^{(i)}$ attained from (MP) may not be the optimal. Hence, when it is not optimal, there exists

---

**Algorithm 1:** Successive Scenario Generation Method.

**Input:** Base load: $p_{i,t}^d$; EV parameters: $E_n, T_{n,k}^{tr}, \eta_{n,t}$.
**Output:** Charging rate $\pi_{k,t}$; Charging choice $I_{n,k,t}$.

1  Initialization: $i \leftarrow 0$, tolerance $\Delta$, upper/lower bound $Z^{ub} \leftarrow +\infty, Z^{lb} \leftarrow -\infty$;
2  Formulate the MP and SP.
3  Solve MP, get $\pi_{k,t}^{(0)}$ and $Z^{lb}$; slove SP with $\pi_{k,t}^{(0)}$, get $I_{n,k,t}^{(0)}$ for $n \in \Phi_w^{(0)}$ and $Z^{ub}$; calculate $Gap = Z^{ub} - Z^{lb}$; set $i \leftarrow 1$.
4  **while** $i \leq N_i$ or $Gap \geq \Delta$ **do**
5      Add worst-case uncontrollable charging load to the base load; solve MP with $I_{n,k,t}$ for $n \in \Phi \backslash \Phi_w^{(i-1)}$, get $\pi_{k,t}^{(i)}$, $I_{n,k,t}^{(i)}$ for $n \in \Phi_b^{(i)}$ and $Z_{(i)}^{lb}$; if $Z_{(i)}^{lb} \geq Z^{lb}, Z^{lb} \leftarrow Z_{(i)}^{lb}$;
6      Slove SP with $\pi_{k,t}^{(i)}$, get $I_{n,k,t}^{(i)}$ for $n \in \Phi_w^{(i)}$ and $Z_{(i)}^{ub}$; if $Z_{(i)}^{ub} \leq Z^{ub}, Z^{ub} \leftarrow Z_{(i)}^{ub}$;
7      Calculate $Gap = Z^{ub} - Z^{lb}$;
8      Update $i \leftarrow i + 1$;
9  **end**

---

a new set of charging choice $I_{n,k,t}'$ that satisfy

$$f^*(\boldsymbol{P}, I_{n,k,t}') \leq f(\boldsymbol{P}, I_{n,k,t}^*) = Z^{ub}. \quad (49)$$

In the meantime, $I_{n,k,t}^*$ attained from (MP) towards optimism. For any other choice $I_{n,k,t}''$ of EVs, we have

$$f^*(\boldsymbol{P}, I_{n,k,t}'') \geq f(\boldsymbol{P}, I_{n,k,t}^*) = Z^{lb}. \quad (50)$$

Therefore, $Z^{ub} - Z^* \leq \Delta$. $\qquad \square$

The algorithm works efficiently. However, it may give a local optimal solution. We are working on an approach to finding the global one.

## IV. CASE STUDY

This section presents the implementation of the proposed LToU dynamic pricing scheme on an interdependent 69-node distribution system and 45-node transportation system, as shown in Fig.2 and Fig.3, to demonstrate its performance. FCSs labeled by the same color are located at road intersections 13, 21, 25, and 34, connecting with nodes 23, 35, 42, and 47 in the 69-node PDN. Firstly, the data of the tested system is prepared. Then, cases are conducted based on optimistic and robust LToU pricing schemes to illustrate the effectiveness of robust LToU pricing scheme and SSG algorithm. All case studies are coded in C++ and solved using GUROBI 9.1.2. The program runs on an Intel(R) Xeon(R) Gold-5118 2.3-GHz server with 256G memory.

### A. Data Preparation

In the interdependent system, FCSs are situated at road intersections 13, 21, 25, and 34, which are connected to nodes 23, 35, 42, and 47 in the 69-node power distribution network (PDN). Additionally, a 1MW PV station is integrated into the distribution system at node 12. The capacity factors for each hour within a 24-hour period are presented in Table I. The hourly load demand is derived from case-69 in MATPOWER [40], with the ratio of hourly load to base load (i.e., load in case-69) detailed in Table I, based on the general load profile.

The specific navigation strategy of EVs in the transportation system is beyond the scope of this paper. Therefore, the traveling time to the FCS is assumed to be proportional to the shortest distance. Each FCS is equipped with 10 chargers. Additionally, the battery capacity and the rated charging power of each EV are set to 80 kWh and 80 kW, respectively.
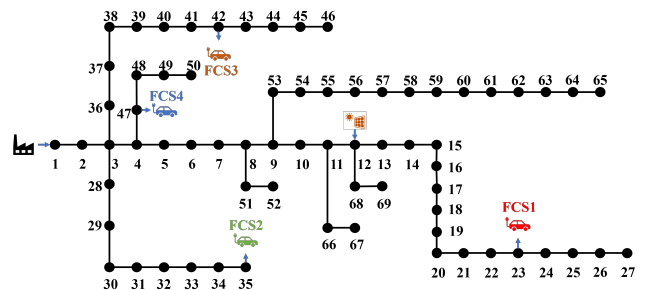


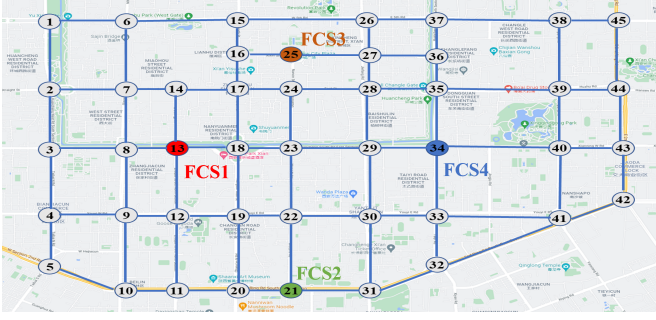Fig. 2. Topology of the 69-node distribution system.

Fig. 3. Map of a 45-node district in Xi'an city.

TABLE I
PV RELATIVE CAPACITY FACTOR AND RELATIVE LOAD RATIO.

| Time slot | Capacity factor | | | | | | Relative load ratio | | | | | |
|---|---|---|---|---|---|---|---|---|---|---|---|---|
| 1-6 | 0.00 | 0.00 | 0.00 | 0.02 | 0.05 | 0.15 | 0.72 | 0.71 | 0.71 | 0.76 | 0.86 | 0.97 |
| 7-12 | 0.32 | 0.54 | 0.70 | 0.83 | 0.97 | 1.00 | 1.03 | 1.04 | 1.05 | 1.05 | 1.03 | 1.01 |
| 13-18 | 0.95 | 0.84 | 0.66 | 0.45 | 0.27 | 0.12 | 1.00 | 0.99 | 0.98 | 0.99 | 1.00 | 1.01 |
| 19-24 | 0.03 | 0.00 | 0.00 | 0.00 | 0.00 | 0.00 | 0.98 | 0.92 | 0.88 | 0.83 | 0.78 | 0.74 |

TABLE II
STEPWISE ELECTRICITY PRICE OF NETWORK INJECTION POWER.

| Power injection (MW) | 0-2.5 | 2.5-3.0 | 3.0-3.5 | 3.5-4.0 | 4.0-$P_{max}$ |
|---|---|---|---|---|---|
| Electricity price ($/MW) | 74.02 | 81.42 | 118.43 | 207.23 | 296.09 |

For simplicity, it is assumed that each FCS can fully charge the EV within one hour. To prevent oligopoly, the average charging rate is set to be $0.15/kWh in each FCS for all time slots in this paper [41]. The discrete charging price map consists of nine equally spaced price points ranging from $0.075/kWh to $0.225/kWh. Stair-like electricity prices are used to calculate the PDN operation cost, which is illustrated in Table.II. Generally, the majority of EV owners exhibit a preference for daytime charging due to its convenience. The discomfort degree for plug-in time is randomly generated, with sampling based on uniform distribution [0, 0.5] from 9:00 to 22:00, and [0.5, 1.5] during the night and early morning, spanning from 23:00 to 8:00. The value of big M is 150. The initial position and SOC of each EV are generated by random simulation.
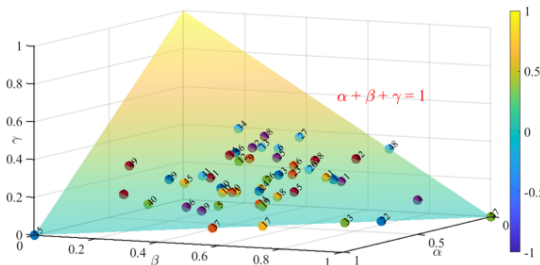


Fig. 4. The sampled attitudes towards to charging fees $\alpha$, travelling cost $\beta$, and plug-in time preference $\gamma$ of 50 EV owners.
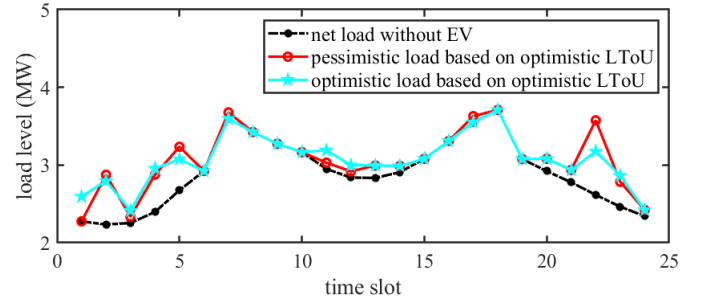


Fig. 5. Net load versus time without considering uncertainty.

## B. Performance of LToU Pricing Scheme

The comfort and satisfaction of the charging process greatly impact the load profile due to the varying responses of customers to charging rate, distance, and plug-in time. The optimal conditions for EV owners are various. Understanding human preference for these factors is critical in designing an effective pricing scheme and efficient load management. With the aim of providing a comprehensive analysis of the attitudes of EV owners towards the charging process, we conduct an exploratory survey involving 500 EV owners in Xi'an, China. Utilizing data collected through a paper-based questionnaire, the preference weights of the samples are distilled into 50 representative points employing the k-means clustering method [42]. The clustering centers serve as resulting samples and are visualized in a three-dimensional scatter plot. All of the samples are located on the plane $\alpha + \beta + \gamma = 1$, and are labeled with their corresponding EV index shown in Fig.4. From the survey results, we can find that EV-27 focuses only on distance, while EV-15 only considers the charging rate. Furthermore, EV-17, -22, -33, and -37 do not consider plug-in time as a priority.
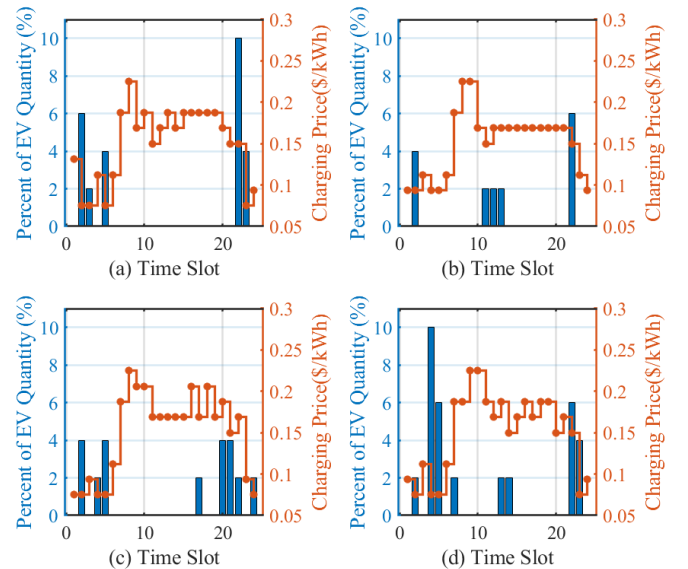


Fig. 6. Charging rate and percent of charging EVs versus time at 4 FCSs based on optimistic LToU.
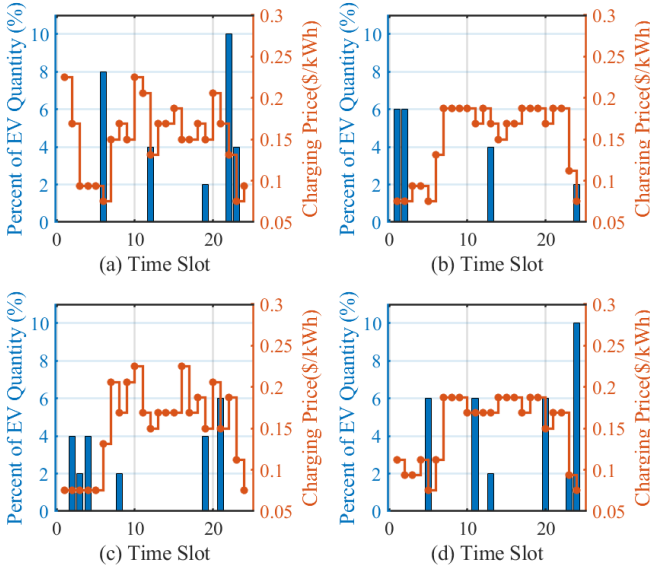
Fig. 7. Charging rate and percent of charging EVs versus time at 4 FCSs based on robust LToU.



Fig. 8. Net load profiles under robust and optimistic LToU.



Fig. 9. The optimality gap of MP and SP.

*1) Necessity of Robust Load Management:* The hourly charging load is partially influenced by the charging rate, making it necessary to investigate the relationship between these two factors. In reality, not all EV owners align their charging decisions with the preferences of the PDN while considering human-choice uncertainty. When some EVs deviate from the optimistic scenario's charging decisions, it significantly impacts the objective value and peak load. This scenario represents the pessimistic scenario, where uncontrollable EVs' choices result in a worst-case upper-level objective.

Fig.5 illustrates the net load curves. The red solid line represents the net load profile with EV demand in the pessimistic scenario, which exhibits a new peak at 22:00 compared to the optimistic scenario due to human-choice uncertainty. Additionally, the objective value rises from \$5,278.3 in the optimistic scenario to \$5,290.7 in the pessimistic scenario. Therefore, it is crucial to propose a robust LToU pricing scheme that aims to flatten the net load curve by partially managing the EV loads.

*2) Effectiveness of Load Management:* To demonstrate the viability of the proposed model and algorithm for managing the EV load and flattening the duck curve, we conduct cases with 50 EVs, 30 controllable and 20 uncontrollable EVs, across 24 time slots. The individual preference weights of each customer are obtained through questionnaires. We compare the proposed robust LToU with the optimistic LToU below:

- Optimistic LToU pricing scheme for EV load management, in which the problem MP is solved only once.
- Robust LToU pricing scheme for EV load management, in which MP and SP are solved iteratively by algorithm 1. Add the top 70% worst-case uncontrollable charging loads to the base load in each iteration.

Fig.6 and Fig.7 present the hourly charging rate and number of EVs charging over time for all FCSs based on the optimistic and robust LToU in the pessimistic scenario, which assumes lower level contributes to a worst upper-level objective. Fig.6
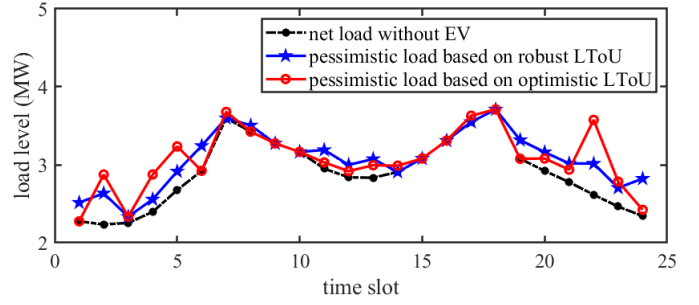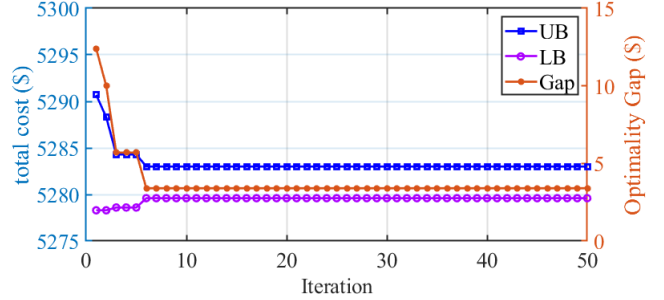
shows that many EVs are charging during the shoulder-price and off-peak-price periods under the optimistic LToU price scheme. However, many EVs charge at the non-lowest-price slot at 22:00 across all four stations forming a new peak because of human-choice uncertainty. In Fig.7, it is observed that few EVs charge at 22:00 in FCS-2, -3, and -4 when charging rates are high, and only 10% of EVs charge at 22:00 in FCS-1. Additionally, an interesting observation is that some EVs charge during periods with non-lowest prices. For example, 6% of EVs are charging in FCS-4 at 20:00 although the prices are not the lowest. This is because these EVs prioritize their preferred plug-in-time over charging fees. The results suggest that the robust LToU pricing scheme is more effective in managing EV loads by leveraging location and temporal information.

With the plug-in time and FCS selection information, we can calculate the net load with the added EV load. Fig.8 displays the net load curves. The net load, incorporating PV, without EV loads shows two peaks in the morning and evening, as depicted by the dashed-dotted line. The red solid line represents the optimized net load profile with EV demand based on optimistic LToU, while the blue solid line shows the optimized net load based on robust LToU. It is obvious that a peak load is caused based on optimistic LToU (i.e. 3.576 MW) which is almost equal to the morning peak (i.e. 3.678 MW) and evening peak (i.e. 3.710 MW). By using the proposed robust LToU price-based EV load management scheme, the worst-case new peak is mitigated. Besides, the pessimistic objective value based on robust LToU is \$5,282.0 which is very close to the optimistic scenario.

*3) Convergence Performance of SSG:* To illustrate the convergence of the proposed algorithm, Fig. 9 presents the
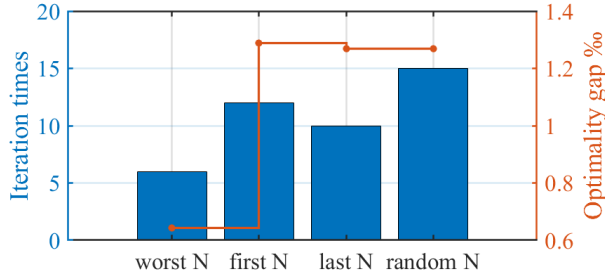
Fig. 10. Performance comparison under different selected EV sequences.

| Uncertainty Range | w/o | Base | +5% | +10% | +15% | +20% |
|---|---|---|---|---|---|---|
| Original Gap | 0 | 2.3‰ | 3.9‰ | 5.5‰ | 6.5‰ | 11.4‰ |
| Optimized Gap | 0 | 1.1‰ | 2.1‰ | 4.0‰ | 4.4‰ | 6.5‰ |
| Iteration Times | - | 6 | 9 | 13 | 14 | 17 |
| Running Time | 7.07s | 45.63s | 78.31s | 117.93s | 125.62s | 133.98s |

optimality gap versus iteration number and the comparison of the total cost of MP and SP. It is noted that the upper and lower bounds are the optimal values of SP and MP respectively. The optimality gap is the difference between the upper bound and lower bound. As shown by the solid line, the optimality gap decreases with iteration in general. After 6 iterations, we observe that both the upper bound and the optimality gap remain unchanged with iteration. Therefore, we conclude that the proposed SSG method requires 6 iterations to achieve a converged solution. The optimality gap reduces by 72.6% (i.e., (12.4-3.4.)/12.4). After it converges, the largest objective violation is $3.4. In other words, the cost in the worst-case scenario is decreased. It indicates that the proposed robust LToU price scheme exhibits robustness.

*4) Effectiveness of Selected Worst EV Sequence:* The SSG method employs the worst $N$ uncertain EVs, which contribute to the peak load from the SP, to generate scenario-related constraints incorporated into the MP. To assess the effectiveness of the scenario generation scheme, simulations are conducted with different EV sequences, including the top worst $N$, the ordered first $N$, the ordered last $N$, and a random selection of $N$. The iteration times and optimality gaps are illustrated in Fig.10. In the proposed scheme, the iteration time is 6, whereas it is 10, 9, and 15 in the first, last, and random schemes, respectively. This discrepancy arises because the selected EVs in other schemes might be charging during valley or shoulder periods contributing less to the pricing process, thereby slowing down the convergence speed. The simulation results indicate that the proposed sequence of the top $N$ worst uncertain EVs exhibits the fastest convergence speed and the smallest optimality gap.

*5) Economic Performance of EV Customer:* In addition to the optimality of the upper-level problem, it is worth considering the economic performance of EV owners in the lower-level problem. For the part of controllable EVs, all EV owners charge at the FCS with the minimum overall cost. However, in the uncontrollable part, some EVs charge at FCSs where the overall cost is not the minimum.

Fig.11 illustrates the objective value associated with different choices for EV-44 in the best and worst scenarios. In the best scenario, it charges at FCS-1 in the 23th time slot, resulting in a cost of 0.424. Conversely, in the worst scenario, EV-44 charges at FCS-1 in the 6th time slot, incurring a cost of 0.434. Although the objective is not the minimum, it still falls within a near optimality for $\delta_{44}$. The numerical results

demonstrate that the proposed robust LToU pricing scheme effectively manages the EV load while ensuring the economic performance of EV owners.

*C. Scalability of Human-choice Uncertainty Model*

*1) Extension to Time-dependent Traveling Time Scene:* Moreover, considering the shortest path, the traveling time varies due to time-dependent traffic congestion. To assess the effectiveness of the proposed model, we extend the cases to include scenarios with time-dependent traveling times. Consequently, we reformulate human choice as a function of traveling time rather than distance, expressed as

$$C_{n,k,t}(\pi) = \alpha\pi_{k,t}E_n + \beta T_{n,k,t}^{tr} + \gamma\eta_{n,t}, \qquad (51)$$

in which, $T_{n,k,t}^{tr}$ is the time-dependent traveling time.

In Fig.12, the net load curves in the time-dependent traveling time scenario are presented. The peak load based on the robust LToU at 18:00 is 3.710 MW, which is lower than the peak load based on the optimistic LToU at 16:00, which is 3.790 MW. As previously established, the proposed robust LToU pricing scheme mitigates the worst-case peak load. Furthermore, the iteration times in the two cases are 6 and 5, respectively. Thus, we can infer that the robust LToU pricing scheme also contributes to flattening the net load curve by effectively managing EV loads in the time-dependent traveling time scenario.

*2) Impact of Human-choice Uncertainty Range:* Based on the proposed human-choice uncertainty model, we observe an expansion in the uncertain choice region of EV owners as the uncertainty range increases. To analyze the effects of distinct uncertainty ranges on the performance of the proposed method, we conduct simulations under various scenarios: cases without uncertainty, those with base uncertainty obtained through a questionnaire, and those with a 5%-20% uncertainty increase. The detailed results are presented in Table III. The findings indicate that iteration times, running time, and optimality gaps increase with a larger uncertainty range. This suggests that EV owners with a broader uncertainty range become less sensitive to price, thus unveiling a limitation in price-based EV load management.

*3) Impact of Uncertain Charging EV Quantity:* To further validate the effectiveness of the proposed near-optimal searching algorithm, we conduct experiments with different levels of uncertainty in the number of charging EVs. Table IV presents the optimality gap and iteration times for each case with varying levels of uncertainty. The results show that the proposed
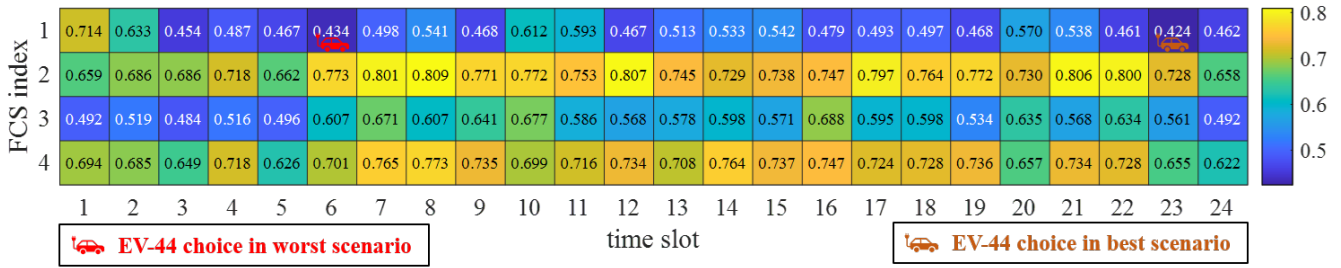
Fig. 11. Costs of different choices for EV-44. EV-44 chooses to charge at time 5 and time 24 in FCS-1 under the worst and best scenarios respectively.
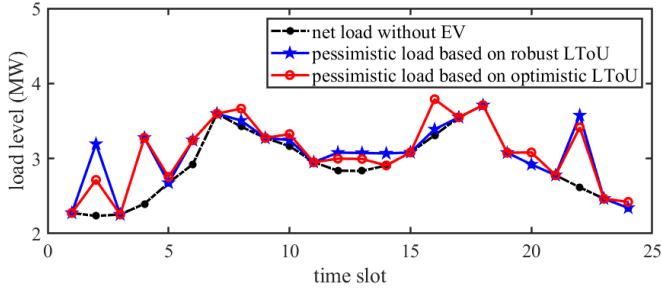


Fig. 12. Comparison of net load profiles under robust and optimistic LToU considering traveling time rather than distance.

TABLE IV
PERFORMANCE UNDER DIFFERENT UNCERTAIN CHARGING EV QUANTITIES.

| Uncertain Quantity | 20% | 40% | 60% |
|---|---|---|---|
| Original Gap | 0.3‰ | 2.3‰ | 7.7‰ |
| Optimized Gap | 0.1‰ | 1.1‰ | 4.8‰ |
| Iteration Times | 2 | 6 | 13 |

TABLE V
THE MODEL SCALE OF TWO DETERMINISTIC OC CASES.

| OC | # Cons. | Non-zeros | Continuous | Integer | # Var. |
|---|---|---|---|---|---|
| OC1 | 486,334 | 1,458,680 | 18,384 | 5,760 | 24,144 |
| OC2 | 49,584 | 153,130 | 23,234 | 5,760 | 28,994 |

algorithm achieves a reduction in the optimality gap, with a reduction of 66.7% in cases with 20% uncertain EVs. Even in cases with higher levels of uncertainty, when the uncertain EV quantity equals 60%, the algorithm still achieves a substantial reduction in the optimality gap, approximately 37.7%. These findings indicate that the proposed algorithm is effective in addressing the challenges posed by this particular type of pessimistic bi-level mixed-integer programming problem.

*4) Computational Performance:* In this section, our main focus is to evaluate the computational performance of the optimality condition models introduced in Section III. After analyzing the model, we have found that the most time-consuming part is the large number of optimality condition constraints. We label the optimality conditions in *proposition 1* and *proposition 3* as **OC1** and **OC2**, respectively.

Table V presents the scale of the models for two cases with

TABLE VI
THE COMPUTATIONAL TIME OF EACH MODEL WITH DIFFERENT EVS.

| Model | EV number | | | |
|---|---|---|---|---|
| | 50 | 100 | 150 | 200 |
| OC1 | 39.65s | 85.55s | 219.47s | 675.68s |
| OC2 | 2.97s | 32.34s | 87.17s | 252.38s |

50 EVs. It is observed that the number of constraints with OC1 is significantly higher than with OC2. For instance, the number of constraints in OC1 is 486,334, while it is 49,584 in OC2. However, it is noted that the number of continuous variables with OC2 is slightly higher than with OC1 due to the newly added ancillary variables. Additionally, the number of integer variables for the two OC methods is the same in the same case, as they are the charging-choice and price-map indicators.

To compare the efficiency of two OCs, we conduct four cases, namely case-1 to case-4, with 50, 100, 150, and 200 EVs, respectively. Table VI presents the computational times for four cases with two different optimality condition methods in the deterministic models. The results show that the computation time of the model with OC2 is much less than that of OC1 in all cases. Furthermore, the computation time of the model with OC1 increases dramatically with the scale of the problem, whereas the time consumed in the model with OC2 increases slowly. The results indicate that the proposed optimality conditions (OC2) method is effective in reducing computational burden.

*5) Impact of Different Demand Levels:* To analyze the system performance under varying demand levels, we conducted simulations with 50, 100, 200, 300, 400, and 500 charging EVs. The results, encompassing iteration times, running time, and optimality gaps, are presented in Table VII. It is observed that both the optimistic and robust optimality gaps increase with a larger quantity of EVs, owing to the corresponding increase in uncertain charging choices. Furthermore, the proposed algorithm requires more iteration times and running time due to the enlarged model scale. Notably, even with 500 EVs, the robust LToU approach reduces the optimality gap from 97.1‰ to 16.0‰ within 2 hours. This indicates that our method can achieve a near-optimal solution within a reasonable running time and optimality gap, even with a higher number of EVs.

| EV Quantity | 50 | 100 | 200 | 300 | 400 | 500 |
|---|---|---|---|---|---|---|
| Original Gap | 2.3‰ | 10.8‰ | 20.7‰ | 41.6‰ | 65.3‰ | 97.1‰ |
| Optimized Gap | 0.2‰ | 4.4‰ | 7.2‰ | 9.5‰ | 13.4‰ | 16.0‰ |
| Iteration Times | 6 | 9 | 12 | 14 | 17 | 21 |
| Running Time | 45.6s | 218.3s | 1062.2s | 2319.1s | 3823.5s | 6249.3s |



Fig. 13. Nodal voltage based on optimistic LToU.
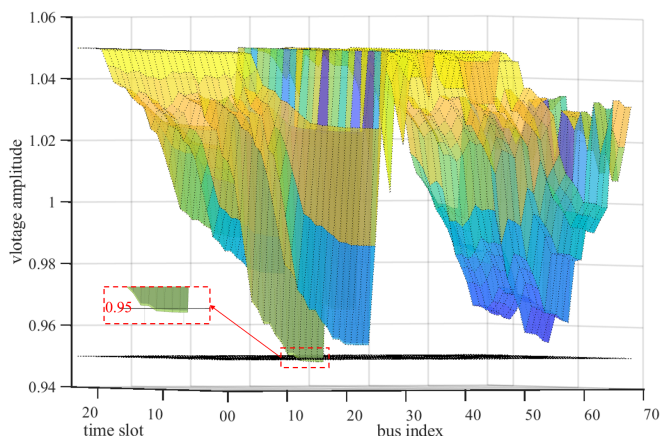


Fig. 14. Nodal voltage based on robust LToU.

*6) Voltage Security Analysis:* The widespread integration of EVs poses the risk of undervoltage challenges in the distribution system. Analyzing the impact of human-choice uncertainty on nodal voltage becomes crucial. To affirm the effectiveness of the proposed method, we enhance the chargers in each FCS to 30 and the total charging EVs to 400. Subsequently, the voltage profiles of the distribution system, both with and without the robust method, are depicted in Fig. 13 and 14.

Here, the worst-case scenario is the uncertain charging choices leading to the lowest voltage. Fig.13, shows that the voltages from node-23 to node-27 at 10:00 fall below the secure voltage limit (i.e., 0.95). The lowest voltage magnitude is 0.948 based on optimistic LToU, highlighting that neglecting human-choice uncertainty may lead to undervoltage. Conversely, by accounting for human-choice uncertainty, the lowest voltage magnitude based on robust LToU is 0.956, as shown in Fig.14. This implies that undervoltage does not occur under robust LToU, underscoring the robustness of robust LToU in addressing human-choice uncertainty.

## V. CONCLUSION

This work presents a robust LToU price-based optimization model to manage EV load considering human-choice uncertainties. A bi-level programming model is developed to formulate the optimal power flow model and mimic the EV's charging behavior. It attacks the low-level human-choice uncertainty, which is still an open question in the community. By establishing a group of near-optimality conditions for the lower level problem, we model a feasible region rather than a point for human behaviors, and propose a successive scenario generation algorit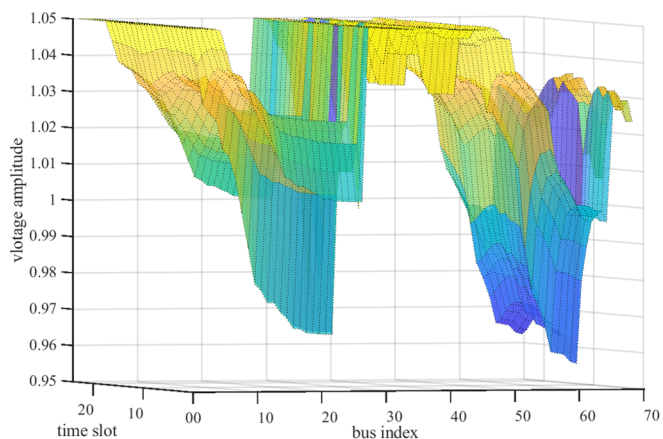hm to solve the problem. The simulation results show that the robust LToU pricing scheme can partially incentivize EVs to charge at desired nodes and time, effectively managing the load.

For future work, we will consider more detailed models in the transportation sector, including vehicle-to-grid and traffic. Besides, we are working on different approaches to attacking low-level uncertainties in the robust bi-level models.

## REFERENCES

[1] U. EIA, "Monthly energy review," report, U.S. Energy Information Administration (EIA), 2022.
[2] IEA, "Global ev outlook 2023," report, International Energy Agency (IEA), 2023.
[3] T. Qian, C. Shao, X. Li, X. Wang, and M. Shahidehpour, "Enhanced coordinated operations of electric power and transportation networks via ev charging services," *IEEE Transactions on Smart Grid*, vol. 11, no. 4, pp. 3019–3030, 2020.
[4] W. Lee, R. Schober, and V. W. S. Wong, "An analysis of price competition in heterogeneous electric vehicle charging stations," *IEEE Transactions on Smart Grid*, vol. 10, no. 4, pp. 3990–4002, 2019.
[5] W. Wei, S. Mei, L. Wu, M. Shahidehpour, and Y. Fang, "Optimal traffic-power flow in urban electrified transportation networks," *IEEE Transactions on Smart Grid*, vol. 8, no. 1, pp. 84–95, 2017.
[6] C. Shao, X. Wang, M. Shahidehpour, X. Wang, and B. Wang, "Partial decomposition for distributed electric vehicle charging control considering electric power grid congestion," *IEEE Transactions on Smart Grid*, vol. 8, no. 1, pp. 75–83, 2017.
[7] S. Lv, Z. Wei, S. Chen, G. Sun, and D. Wang, "Integrated demand response for congestion alleviation in coupled power and transportation networks," *Applied Energy*, vol. 283, p. 116206, 2021.
[8] D. Wu, D. C. Aliprantis, and L. Ying, "Load scheduling and dispatch for aggregators of plug-in electric vehicles," *IEEE Transactions on Smart Grid*, vol. 3, no. 1, pp. 368–376, 2012.
[9] G. Zhang, S. T. Tan, and G. G. Wang, "Real-time smart charging of electric vehicles for demand charge reduction at non-residential sites," *IEEE Transactions on Smart Grid*, vol. 9, no. 5, pp. 4027–4037, 2018.
[10] H. S. Jang, K. Y. Bae, B. C. Jung, and D. K. Sung, "Apartment-level electric vehicle charging coordination: peak load reduction and charging payment minimization," *Energy and Buildings*, vol. 223, p. 110155, 2020.
[11] K. Zhou, L. Cheng, L. Wen, X. Lu, and T. Ding, "A coordinated charging scheduling method for electric vehicles considering different charging demands," *Energy*, vol. 213, p. 118882, 2020.
[12] S. S. Shuvo and Y. Yilmaz, "Demand-side and utility-side management techniques for increasing ev charging load," *IEEE Transactions on Smart Grid*, vol. 14, no. 5, pp. 3889–3898, 2023.
[13] W. Wu, Y. Lin, R. Liu, and W. Jin, "The multi-depot electric vehicle scheduling problem with power grid characteristics," *Transportation Research Part B: Methodological*, vol. 155, pp. 322–347, 2022.

[14] A. Ghosh and V. Aggarwal, "Menu-based pricing for charging of electric vehicles with vehicle-to-grid service," *IEEE Transactions on Vehicular Technology*, vol. 67, no. 11, pp. 10268–10280, 2018.

[15] A. Moradipari, N. Tucker, and M. Alizadeh, "Mobility-aware electric vehicle fast charging load models with geographical price variations," *IEEE Transactions on Transportation Electrification*, vol. 7, pp. 554–565, JUN 2021.

[16] I. S. Bayram and S. Galloway, "Pricing-based distributed control of fast ev charging stations operating under cold weather," *IEEE Transactions on Transportation Electrification*, vol. 8, pp. 2618–2628, JUN 2022.

[17] W. Kong, H. Ye, N. Wei, D. Xing, and W. Chen, "Dynamic pricing based EV load management in distribution network," *Energy Reports*, vol. 8, pp. 798–805, Aug. 2022. ICPE 2021 - The 2nd International Conference on Power Engineering.

[18] A. Moradipari and M. Alizadeh, "Pricing and routing mechanisms for differentiated services in an electric vehicle public charging station network," *IEEE Transactions on Smart Grid*, vol. 11, no. 2, pp. 1489–1499, 2020.

[19] C. Luo, Y.-F. Huang, and V. Gupta, "Stochastic dynamic pricing for ev charging stations with renewable integration and energy storage," *IEEE Transactions on Smart Grid*, vol. 9, no. 2, pp. 1494–1505, 2018.

[20] N. A. El-Taweel, H. Farag, M. F. Shaaban, and M. E. AlSharidah, "Optimization model for ev charging stations with pv farm transactive energy," *IEEE Transactions on Industrial Informatics*, vol. 18, no. 7, pp. 4608–4621, 2022.

[21] W. Wu, Y. Lin, R. Liu, Y. Li, Y. Zhang, and C. Ma, "Online ev charge scheduling based on time-of-use pricing and peak load minimization: Properties and efficient algorithms," *IEEE Transactions on Intelligent Transportation Systems*, vol. 23, no. 1, pp. 572–586, 2022.

[22] M. Besançon, M. F. Anjos, L. Brotcorne, and J. A. Gómez-Herrera, "A bilevel approach for optimal price-setting of time-and-level-of-use tariffs," *IEEE Transactions on Smart Grid*, vol. 11, no. 6, pp. 5462–5465, 2020.

[23] S. González, F. Feijoo, F. Basso, V. Subramanian, S. Sankaranarayanan, and T. K. Das, "Routing and charging facility location for evs under nodal pricing of electricity: A bilevel model solved using special ordered set," *IEEE Transactions on Smart Grid*, vol. 13, no. 4, pp. 3059–3068, 2022.

[24] B. Zeng and Y. An, "Solving bilevel mixed integer program by reformulations and decomposition," *Optimization Online*, pp. 1–34, 2014.

[25] O. Tavaslıoğlu, O. A. Prokopyev, and A. J. Schaefer, "Solving stochastic and bilevel mixed-integer programs via a generalized value function," *Operations Research*, vol. 67, no. 6, pp. 1659–1677, 2019.

[26] D. Bertsimas, E. Litvinov, X. A. Sun, J. Zhao, and T. Zheng, "Adaptive robust optimization for the security constrained unit commitment problem," *IEEE Transactions on Power Systems*, vol. 28, no. 1, pp. 52–63, 2013.

[27] Z. Ding, X. Huang, Z. Liu, and Z. Zhang, "A two-level scheduling algorithm for battery systems and load tap changers coordination in distribution networks," *IEEE Transactions on Power Delivery*, vol. 37, no. 4, pp. 3027–3037, 2022.

[28] A. Le Rhun, F. Bonnans, G. De Nunzio, T. Leroy, and P. Martinon, "A bilevel energy management strategy for hevs under probabilistic traffic conditions," *IEEE Transactions on Control Systems Technology*, vol. 30, no. 2, pp. 728–739, 2022.

[29] C. Feng, Y. Wang, K. Zheng, and Q. Chen, "Smart meter data-driven customizing price design for retailers," *IEEE Transactions on Smart Grid*, vol. 11, no. 3, pp. 2043–2054, 2020.

[30] C. Le Floch, F. Belletti, and S. Moura, "Optimal charging of electric vehicles for load shaping: A dual-splitting framework with explicit convergence bounds," *IEEE Transactions on Transportation Electrification*, vol. 2, pp. 190–199, JUN 2016.

[31] J. Hu, C. Si, M. Lind, and R. Yu, "Preventing distribution grid congestion by integrating indirect control in a hierarchical electric vehicles' management system," *IEEE Transactions on Transportation Electrification*, vol. 2, pp. 290–299, SEP 2016.

[32] Y. O. Assolami, A. Gaouda, and R. El-shatshat, "Impact on voltage quality and transformer aging of residential prosumer ownership of plug-in electric vehicles: Assessment and solutions," *IEEE Transactions on Transportation Electrification*, vol. 8, pp. 492–509, MAR 2022.

[33] M. Besançon, M. F. Anjos, and L. Brotcorne, "Robust Bilevel Optimization for Near-Optimal Lower-Level Solutions," Jan. 2023. arXiv:1908.04040 [cs, math].

[34] B. Zeng, "Easier than we thought - a practical scheme to compute pessimistic bilevel optimization problem," *Social Science Research Network*, 2015.

[35] B. Zeng and L. Zhao, "Solving two-stage robust optimization problems using a column-and-constraint generation method," *Operations Research Letters*, vol. 41, no. 5, pp. 457–461, 2013.

[36] J. Luo, L. Rao, and X. Liu, "Spatio-temporal load balancing for energy cost optimization in distributed internet data centers," *IEEE Transactions on Cloud Computing*, vol. 3, no. 3, pp. 387–397, 2015.

[37] C. Joe-Wong, I. Kamitsos, and S. Ha, "Interdatacenter job routing and scheduling with variable costs and deadlines," *IEEE Transactions on Smart Grid*, vol. 6, no. 6, pp. 2669–2680, 2015.

[38] E. M. L. Beale and J. J. H. Forrest, "Global optimization using special ordered sets," *Mathematical Programming*, vol. 10, pp. 52–69, Dec. 1976.

[39] Z. Yang, H. Zhong, A. Bose, T. Zheng, Q. Xia, and C. Kang, "A linearized opf model with reactive power and voltage magnitude: A pathway to improve the mw-only dc opf," *IEEE Transactions on Power Systems*, vol. 33, no. 2, pp. 1734–1745, 2018.

[40] C. E. M.-S. R. D. Zimmerman, "MATPOWER (7.1) [Software]." 2020.

[41] NERL, "Research determines financial benefit from driving electric vehicles." https://www.nrel.gov/news/press/2020/research-determines-financial-benefit-from-driving-electric-vehicles.html#. June, 2020.

[42] Wikipedia contributors, "K-means clustering — Wikipedia, the free encyclopedia," 2023. [Online; accessed 27-January-2024].

**Weile Kong** received the B.S. degree in automation from Xi'an Jiaotong University, China, in 2020. He is currently working towards Ph.D. in Electrical Engineering, Xi'an Jiaotong University. His research interests include demand response, vehicle-to-grid, and optimal control in power systems.

**Hongxing Ye** (SM'17) received the B.S. and M.S. degree from Xi'an Jiaotong University (XJTU), Xi'an, China, and the Ph.D. degree from the Illinois Institute of Technology, Chicago, IL, USA, in 2016, all in Electrical Engineering. He is currently a Professor in Dep. of Automation, XJTU. He was a tenure-track assistant professor at Cleveland State University, Cleveland, USA, before joining XJTU. His research interests include power system operation, vehicle-to-grid, and data-driven optimization in cyber-physical system.
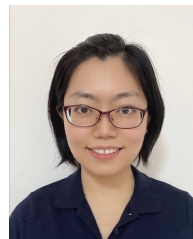
**Yinyin Ge** received the B.S. degree in automation and the M.S. degree in systems engineering from Xi'an Jiaotong University (XJTU), China, in 2008 and 2011, respectively, and the Ph.D. degree in electrical engineering from the Illinois Institute of Technology, Chicago, in 2016. She is currently an Associate Professor at XJTU. She was a Research Associate with Case Western Reserve University before joining XJTU. Her research interests include demand response, power system resilience, PMU applications in smart grid, monitoring, visualization, and state estimation for distribution systems.